Available online at www.sciencedirect.com
ScienceDirect
Journal of Sound and Vibration 308 (2007) 12–27
JOURNAL OF SOUND AND VIBRATION
www.elsevier.com/locate/jsvi

Vibration of beams with arbitrary discontinuities and boundary conditions

Jialai Wang[a,*], Pizhong Qiao[b,c]

[a]Department of Civil, Construction, and Environmental Engineering, The University of Alabama Tuscaloosa, AL 35487-0205, USA
[b]Department of Civil and Environmental Engineering, Washington State University, Pullman, WA 99164-2910, USA
[c]Integrated Smart Structures, Inc., 2601 Twin Creeks Dr., Copley, OH 44321-1770, USA

Received 23 August 2005; received in revised form 5 October 2006; accepted 15 June 2007
Available online 4 September 2007

Abstract

A general solution of the vibration of an Euler–Bernoulli beam with arbitrary type of discontinuity at arbitrary number of locations is presented in this paper. To account for the discontinuity term induced by various additional elements on the beam, Heaviside's function is used to express the modal displacement of the whole beam by a single function. This general modal displacement function is then solved by using Laplace transformation. This general solution consists of four types of basic modal shapes induced by four corresponding types of discontinuity terms at the discontinuity points. Various discontinuity terms are obtained and expressed by the boundary values of the modal displacement in a recursive way. Consequently, the modal displacement can be determined by examining only the conditions on the boundary. In such a way, the present solution reduces the vibration of beams with arbitrary discontinuities to the same order of the case without discontinuity point. To demonstrate the efficiency and applicability of the present method, three application examples are presented. Calculation example shows that the lead–zirconate–titanate (PZT) actuator should be placed as close to the fixed end as possible to achieve the best excitation effect on a cantilever beam. A new method to calculate the driving-point anti-resonance frequency is also proposed. Numerical results suggest that the variation of driving-point anti-resonance frequency can be used to determine the location and size of crack in beams. Due to the generic nature of the solution and the problem, the present method can be utilized in smart structures modeling and structural health monitoring of beam-type structures.

1. Introduction

Structural health monitoring is one of the most important keys in maintaining safety and integrity of structures and avoiding loss of human life and/or monetary loss due to the catastrophic failure of structures. Among many structural health-monitoring techniques, the dynamic response-based damage detection method [1] attracts most attention due to its simplicity for implementation. This technique makes use of the dynamic response of structures, which offers unique information on the defects contained with these structures. Changes in the physical properties of the structures due to damage can alter the dynamic response, such as the

*Corresponding author. Tel.: +1 205 348 6786; fax: +1 205 348 0783.
E-mail address: JWang@eng.ua.edu (J. Wang).

0022-460X/$ - see front matter © 2007 Elsevier Ltd. All rights reserved.
doi:10.1016/j.jsv.2007.06.071

natural frequency and mode shape. These physical parameter changes can be extracted to predict damage information, such as the presence, location and severity of damage in a structure.

As a basis of dynamics-based structural health monitoring technique, free vibration of beams with cracks has been under extensive examination in the last three decades [1–7]. Many crack models have been proposed in the literature to simulate the effect of cracks on the dynamic behavior of beams [7]. A thorough survey of the state-of-the-art of the vibration of cracked structures was given by Diamarogonas [7]. Among those crack models, local flexibility model is used most widely. In this model, the local flexibility induced by a transverse edge crack to the beam is simulated by a rotational spring at the location of the crack [2]. The stiffness of this spring is evaluated by use of fracture mechanics method [2]. In this way, a discontinuity of slope is introduced at the location of the crack. To formulate the free vibration of the cracked beam, a common approach used in the literature is to divide the beam into two sub-beams and different modal displacement functions are used for each sub-beam. As shown in the following text, the governing equation of modal displacement for an Euler–Bernoulli beam is fourth order. Therefore, eight unknown coefficients exist in the expressions of modal displacement of the cracked beam (four for each sub-beam) [2,3]. To determine these unknowns, four boundary conditions and four continuity conditions at the location of the crack have to be employed. As a result, the eigenvalue equation of the problem is expressed as an eighth-order determinant equated to zero. In the case of n cracks in the beam, the order of the determinant increases to $4(n+1)$ [3]. It is extremely difficult to find the root of such a higher-order transcendental equation. Therefore, recent research focused on finding more efficient approaches to simulate the free vibration of beams with multiple cracks. Shifrin and Ruotolo [4] developed a new method which reduces the order of the determinant for a beam with n cracks from order of $4(n+1)$ drastically to order of $(n+2)$. Based on this approach, Li [5] further reduced the determinant to order of 2 through a recursive formula. By using the transfer matrix method, Khibm and Lien [6] reduced the order of the determinant to order of 4. It should be pointed out that the local flexibility method adopted in above studies suffers from many limitations. As discussed in detail by Dimarogonas and Chondos [8] and Chondros [9], it is difficult to relate flaw position and size with stiffness change due to the fact that the crack-induced modification of the stress field decays with the distance from the crack.

The above studies are limited to the case of transverse crack (rotational spring), which is just one of many types of discontinuities for beams. In civil and mechanical engineering, there are many types of additional elements such as intermediate resilient support, rigid or elastic spring-mass system, internal hinge, etc., or any arbitrary combination of them, existing at several locations along a beam. At the locations of these additional elements, different discontinuities are induced complicating the analysis of the vibration of the beam. Similar to the case of multiple cracked beam, Bapat and Bapat [10] found that the eignevalue equation for a beam with n additional elements is given by letting a $4(n+1)$th-order determinant to be zero. To avoid the difficulty encountered in solving higher order eigenvalue equation, the approximated methods were usually employed in the literature [11–15]. By using a group of fundamental solutions for a segment of beam, Li [16] presented an analytical solution to the free vibration of nonuniform beams for several discontinuity cases. This method was essentially an extension of Shifrin and Ruotolo's approach [4].

It should be pointed out that there is only one discontinuity for most additional elements studied in the literature. For instance, only the slope is discontinuous at the location of an elastic rotational spring; while other parameters, such as deflection, curvature and the shear force are continuous. Shifrin and Ruotolo's approach [4] took the advantage of this feature and accounted for only the discontinuity term by using general functions (Heaviside or Dirac delta function). While in a conventional approach outlined in Ref. [3], four continuity conditions were established at each discontinuity point. Obviously, three of them (continuity conditions of displacement, curvature (bending moment), and the third order derivative of the displacement (shear force)) are redundant.

Although the solutions are available in the literature for the vibration of beams with some special discontinuities, there is no general solution to account for arbitrary combinations of discontinuities and boundary conditions. In this study, an attempt is made to develop such a solution. Similar to Shifrin and Ruotolo's approach [4], general functions (Heaviside and Dirac delta functions) are used to account for the discontinuity induced by the additional elements. Unlike in Ref. [3] where different functions are used for each segment of the beam, only a general displacement function is used in this study to describe the whole beam. This general function technique is developed by Yavari [17,18] in studying static response of beams with

multiple discontinuities. It can be seen that the available solutions [4,5,16] are special cases of the present general solution. The present solution can be used conveniently not only to free vibration, but also to forced vibration of beams with arbitrary discontinuities and boundary conditions.

This paper is arranged as follows. The general solution of the modal displacement of a beam with arbitrary discontinuities is derived first using general function. Continuity conditions at the locations of additional elements are then derived for a variety of additional elements on beams. To demonstrate the applicability and efficiency of the general solution, three important problems in smart structures modeling and damage detection are solved by the present method. Some new light shed on the effect of transverse cracks on the dynamic behavior of beams is also discussed.

2. General solution

2.1. Vibration of beams with one discontinuity point

An Euler–Bernoulli beam under general boundary conditions as shown in Fig. 1 is examined in this section. For the convenience of formulation, only one discontinuity point at x_1 is considered on the beam dividing the beam into segments I and II, respectively (Fig. 1). The discontinuity term at this point can be the deflection, slope, curvature, the third order derivative of the deflection, or any combination of above four terms. All four discontinuity terms are considered in the formulation to account for all possible discontinuity configurations at x_1. A commonly used approach to the vibration of this beam is to consider segments I and II separately [2,3]. In this way, the equations of motion of each segment read

$$EIw_1''''(x,t) + \rho A\ddot{w}_1(x,t) = 0, \tag{1}$$

$$EIw_2''''(x,t) + \rho A\ddot{w}_2(x,t) = 0, \tag{2}$$

where $w_1(x,t)$ and $w_2(x,t)$ are the transverse deflections of the segments I and II, respectively; the prime and dot over w_i $(i=1,2)$ are the derivatives of the transverse deflection with respect to x and t, respectively; E and I are the Young's modulus and moment inertia of the beam; ρ and A are the density and cross-section area of the beam, respectively. Noting that Eqs. (1) and (2) are the fourth order differential equations, four boundary and four continuity conditions at x_1 are needed to determine eight coefficients of the modal deflection functions (i.e., $w_1(x,t)$ and $w_2(x,t)$). If there are n discontinuity points on the beam, the total number of coefficients to be determined becomes $4(n+1)$, which leads to solve $4(n+1)$ equations simultaneously [3,10]. In such a case, the difficulty in calculation increases dramatically and "in general … can be very complex even for $n=2$" as pointed out by Gugoze [19]. To avoid this difficulty, an alternative approach is developed in this study in which the deflection of the whole beam is expressed in term of a single function. To facilitate this aim, let

$$\Delta w(x,t) = w_2(x,t) - w_1(x,t), \tag{3}$$

then

$$w(x,t) = w_1(x,t) + \Delta w(x,t)H(x-x_1), \tag{4}$$

where $w(x,t)$ is the deflection function of the whole beam, which is a generalized function with discontinuities at location x_1. $H(x-x_1)$ is Heaviside function which jumps from zero to unit at location x_1. Differentiating

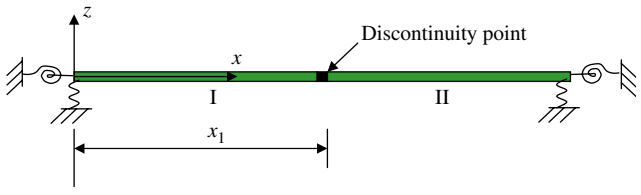

Fig. 1. An Euler–Bernoulli beam with single discontinuity point at x_1.

both sides of Eq. (4) with respect to x, we have

$$w'(x,t) = w_1'(x,t) + \Delta w'(x,t)H(x-x_1) + \Delta w(x_1,t)\delta(x-x_1), \tag{5}$$

$$w''(x,t) = w_1''(x,t) + \Delta w''(x,t)H(x-x_1) + \Delta w'(x_1,t)\delta(x-x_1) + \Delta w(x_1,t)\delta'(x-x_1) \tag{6}$$

$$\begin{aligned} w'''(x,t) = {} & w_1'''(x,t) + \Delta w'''(x,t)H(x-x_1) + \Delta w''(x_1,t)\delta(x-x_1) + \Delta w'(x_1,t)\delta'(x-x_1) \\ & + \Delta w(x_1,t)\delta''(x-x_1), \end{aligned} \tag{7}$$

$$\begin{aligned} w''''(x,t) = {} & w_1''''(x,t) + \Delta w''''(x,t)H(x-x_1) + \Delta w'''(x_1,t)\delta(x-x_1) + \Delta w''(x_1,t)\delta'(x-x_1) \\ & + \Delta w'(x_1,t)\delta''(x-x_1) + \Delta w(x_1,t)\delta'''(x-x_1), \end{aligned} \tag{8}$$

where $\delta(x-x_1)$ is Dirac delta function. Combining Eqs. (1) and (2) gives

$$w_1''''(x,t) + \frac{\rho A}{EI}\ddot{w}_1(x,t) + \left(w_2''''(x,t) + \frac{\rho A}{EI}\ddot{w}_2(x,t) - \left(w_1''''(x,t) + \frac{\rho A}{EI}\ddot{w}_1(x,t)\right)\right)H(x-x_1) = 0. \tag{9}$$

Rearranging Eq. (9) leads to

$$w_1''''(x,t) + \Delta w''''(x,t)H(x-x_1) = -\frac{\rho A}{EI}(\ddot{w}_1(x,t) + \Delta\ddot{w}(x,t)H(x-x_1)). \tag{10}$$

Substituting Eq. (10) into Eq. (8) yields

$$\begin{aligned} w''''(x,t) + \frac{\rho A}{EI}\ddot{w}(x,t) = {} & \Delta w'''(x_1,t)\delta(x-x_1) + \Delta w''(x_1,t)\delta'(x-x_1) + \Delta w'(x_1,t)\delta''(x-x_1) \\ & + \Delta w(x_1,t)\delta'''(x-x_1). \end{aligned} \tag{11}$$

Eq. (11) gives the equation of motion of the Euler–Bernoulli beam with discontinuities in term of general equation $w(x,t)$.

Considering free vibration or harmonic forced vibration, Eq. (11) can be solved through variable separation method. Let

$$w(x,t) = W(x)\sin(\omega t), \tag{12}$$

where $W(x)$ is the modal displacement of the beam. Substituting Eq. (12) into Eq. (11), we have

$$\begin{aligned} W''''(x) - \frac{\rho A\omega^2}{EI}W(x) = {} & \Delta W'''(x_1)\delta(x-x_1) + \Delta W''(x_1)\delta'(x-x_1) + \Delta W'(x_1)\delta''(x-x_1) \\ & + \Delta W(x_1)\delta'''(x-x_1). \end{aligned} \tag{13}$$

Applying Laplace transform to Eq. (13) yields

$$\begin{aligned} W(s) = {} & \frac{s^3}{s^4-\lambda^4}W(0) + \frac{s^2}{s^4-\lambda^4}W'(0) + \frac{s}{s^4-\lambda^4}W''(0) + \frac{1}{s^4-\lambda^4}W'''(0) + \frac{s^3\,\mathrm{e}^{-sx_1}}{s^4-\lambda^4}\Delta W(x_1) \\ & + \frac{s^2\,\mathrm{e}^{-sx_1}}{s^4-\lambda^4}\Delta W'(x_1) + \frac{s\,\mathrm{e}^{-sx_1}}{s^4-\lambda^4}\Delta W''(x_1) + \frac{\mathrm{e}^{-sx_1}}{s^4-\lambda^4}\Delta W'''(x_1), \end{aligned} \tag{14}$$

where $\lambda = \sqrt[4]{(\rho A\omega^2/EI)}$. Note that

$$\begin{aligned} L^{-1}\left\{\frac{1}{s^4-\lambda^4}\right\} &= \frac{1}{2\lambda^3}(\sinh(\lambda x) - \sin(\lambda x)) = \frac{S_3(\lambda x)}{\lambda^3}, \\ L^{-1}\left\{\frac{s}{s^4-\lambda^4}\right\} &= \frac{1}{2\lambda^2}(\cosh(\lambda x) - \cos(\lambda x)) = \frac{S_2(\lambda x)}{\lambda^2}, \\ L^{-1}\left\{\frac{s^2}{s^4-\lambda^4}\right\} &= \frac{1}{2\lambda}(\sinh(\lambda x) + \sin(\lambda x)) = \frac{S_1(\lambda x)}{\lambda}, \\ L^{-1}\left\{\frac{s^3}{s^4-\lambda^4}\right\} &= \frac{1}{2}(\cosh(\lambda x) + \cos(\lambda x)) = S_0(\lambda x). \end{aligned} \tag{15}$$

The modal displacement $W(x)$ can then be easily obtained by applying inverse Laplace transform on Eq. (14) as

$$W(x) = W(0)S_0(\lambda x) + \frac{W'(0)}{\lambda}S_1(\lambda x) + \frac{W''(0)}{\lambda^2}S_2(\lambda x) + \frac{W'''(0)}{\lambda^3}S_3(\lambda x) + \left(\Delta W(x_1)S_0(\lambda(x-x_1)) + \frac{\Delta W'(x_1)}{\lambda}S_1(\lambda(x-x_1)) + \frac{\Delta W''(x_1)}{\lambda^2}S_2(\lambda(x-x_1)) + \frac{\Delta W'''(x_1)}{\lambda^3}S_3(\lambda(x-x_1))\right)H(x-x_1). \tag{16}$$

2.2. Vibration of beams with multiple discontinuity points

The above formulation for a beam with a single discontinuity point can be easily extended to a beam with multiple discontinuity points as one shown in Fig. 2. In Fig. 2, an Euler–Bernoulli beam is divided into $n+1$ segments by n discontinuity points. These discontinuity points can be caused by an applied pointed shear force, a bending moment, an intermediate support, an attached concentrated mass, or a transverse edged crack on the beam. By using general function, the deflection of the cracked beam can be written as

$$w(x,t) = w_1(x,t) + \sum_{i=1}^{n}(w_{i+1}(x,t) - w_i(x,t))H(x-x_i), \tag{17}$$

where $w_i(x,t)$ is the deflection of the ith segment of the beam; x_i is the location of the ith discontinuity point. Following the similar procedure in the above section, the equation of motion of this beam is obtained as

$$w''''(x,t) + \frac{\rho A}{EI}\ddot{w}(x,t) = \sum_{i=1}^{n}\sum_{j=0}^{3}\left(w_{i+1}^{(j)}(x_i,t) - w_i^{(j)}(x_i,t)\right)\delta^{(3-j)}(x-x_i). \tag{18}$$

By using Eq. (12), the governing equation of mode shape becomes

$$W''''(x) - \frac{\rho A\omega^2}{EI}W(x) = \sum_{i=1}^{n}\sum_{j=0}^{3}\left(W_{i+1}^{(j)}(x_i+) - W_i^{(j)}(x_i-)\right)\delta^{(3-j)}(x-x_i). \tag{19}$$

Following the same approach described in the above section, we have

$$W(x) = \sum_{i=0}^{N}H(x-x_i)\sum_{j=0}^{3}\frac{\Delta W^{(j)}(x_i)}{\lambda^j}S_j(\lambda(x-x_i)). \tag{20}$$

Eq. (20) expresses the modal displacement of the whole beam with n discontinuity points by a single function $W(x)$. In this way, a beam with multiple discontinuity points can be treated as one without any discontinuity point. The difficulty experienced in the commonly used approach [3,10] can thus be avoided. Note that x_1, which is zero in the coordinate system of Fig. 2, is the location of the left boundary of the beam. Eq. (20) suggests that the boundary of the beam is also a discontinuity point of the beam. Each discontinuity term at a given location introduces a basic shape function starting at that point. The total modal displacement of the beam $W(x)$ is essentially the superposition of all these basic functions.

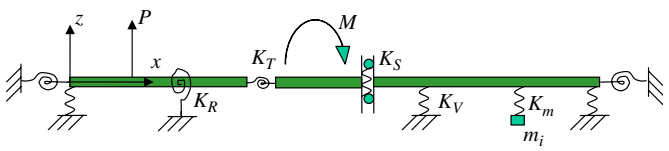

Fig. 2. Euler–Bernoulli beam with multiple discontinuity points.

3. Discontinuities

There are totally $4(n+1)$ unknown discontinuity terms in Eq. (20) to be determined by four boundary and $4n$ continuity conditions (four continuity conditions at each of these n discontinuity points). It rarely occurs that all four possible discontinuity terms exist simultaneously at a discontinuity point. In most practical cases, only one is nonzero at internal discontinuity points and two are nonzero at boundary discontinuity points. If these nonzero discontinuity terms are obtained by the boundary values of the modal displacement, the modal displacement can be simply determined through the boundary conditions as in the case of no discontinuities.

3.1. Concentrated harmonic loads

If a concentrated harmonic force P_i is applied at x_i as shown in Fig. 3(a), the only nonzero discontinuity term is $\Delta W'''(x_i)$. The equilibrium condition at this point requires

$$P(x_i+) - P(x_i-) = P_i. \tag{21}$$

Considering the constitutive law of the Euler–Bernoulli beam, we have

$$W'''_{i+1}(x_i+) - W'''_i(x_i-) = \Delta W'''(x_i) = \frac{P_i}{EI}. \tag{22}$$

Following the similar procedure, the only discontinuity induced by a harmonic concentrated bending moment M_i at x_i (Fig. 3(b)) is given by

$$W''_{i+1}(x_i+) - W''_i(x_i-) = \Delta W''(x_i) = \frac{M_i}{EI}. \tag{23}$$

3.2. Intermediate attachments

Free vibration of an Euler–Bernoulli beam with attachments has been studied by many researchers [10–16,20–22]. Different discontinuities are introduced to the modal displacement by various attachments. Exact solutions available in the literature are quite complex when more than two intermediate attachments are involved [19].

Fig. 4(a) shows an elastic translational spring with stiffness K_{Vi} at x_i, which can be used to simulate the intermediate support of a continuous beam. Due to the deformation of the beam at x_i, a reaction force P_{Ri} is generated at x_i and given by

$$P_{Ri} = K_{Vi} W(x_i). \tag{24}$$

Considering Eq. (22), the only discontinuity term at this location is given by

$$\Delta W'''(x_i) = -\frac{1}{EI} K_{Vi} W(x_i). \tag{25}$$

Specifically, if K_{Vi} is infinite, the elastic support becomes a roller support (Fig. 4(b)). In such a case, $\Delta W'''(x_i)$ cannot be determined by Eq. (25) any more. However, an extra condition at x_i can be used

$$W(x_i) = 0. \tag{26}$$

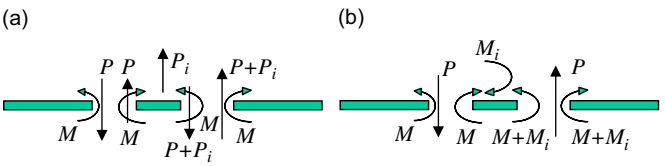

Fig. 3. Discontinuity induced by applied load: (a) concentrated shear force; and (b) concentrated bending moment.

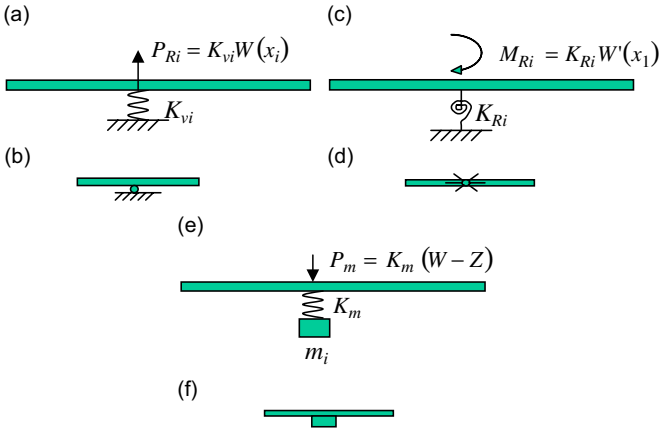

Fig. 4. Discontinuities induced by intermediate attachments: (a) elastic translational spring support; (b) extreme condition of (a) roller support; (c) elastic rotational spring support; (d) extreme condition of (d) fixed rotation; (e) spring–mass system; and (f) concentrated mass particle.

Fig. 4(c) shows an elastic rotational spring existing at x_i. In this case, a reaction bending moment generated by the support at x_i reads

$$M_{Ri} = K_{Ri}W'(x_i). \tag{27}$$

By using Eq. (23), the only discontinuity exists at this point is given by

$$\Delta W''(x_i) = \frac{1}{EI}K_{Ri}W'(x_i). \tag{28}$$

Particularly, if K_{Ri} is infinite (Fig. 4(d)), no rotation is allowed at x_i. In such a case, the discontinuity term cannot be determined by Eq. (29). Instead, we have

$$W'(x_i) = 0. \tag{29}$$

Fig. 4(e) describes a uniform Euler–Bernoulli beam carrying a mass particle at x_i through an elastic spring with stiffness K_m. The free vibration of such a beam has been studied by many researchers [5,11,15,23]. Such a spring-mass system can be replaced by a translational spring with the effective spring constant K_{Vi} given by [23]

$$K_{Vi} = \frac{-K_m m_i \omega^2}{K_m - m_i \omega^2}. \tag{30}$$

The discontinuity is given by Eq. (25). If the concentrated mass m_i is directly attached to the beam, as shown in Fig. 4(f), K_m is infinite. In such a case, K_{Vi} reduces to

$$K_{Vi} = -m_i \omega^2. \tag{31}$$

3.3. Internal elastic connector

The free vibration of cracked beams has been studied extensively during the last decade [1–6,25–27] due to its application in damage detection of beams. Extra local bending and transverse flexibility can be induced at the vicinity of the tip of the transverse crack due to the severe strain energy concentration. A rotational spring shown in Fig. 5(a) is usually used to simulate the effect of the crack on the dynamic behavior of the beam [2]. This model is based on the following assumptions: (a) the crack changes only the stiffness of the beam and the mass of the beam is unchanged, (b) the crack is always open, and (c) only the local bending flexibility is considered and axial and transverse flexibilities are neglected. The stiffness of the spring is determined by relating the local flexibility to the strain energy concentration at the vicinity of the crack tip through the

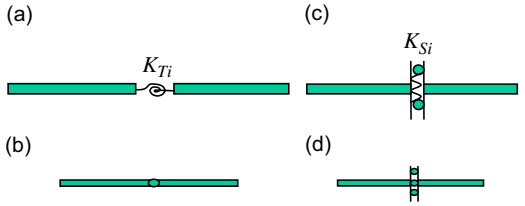

Fig. 5. Internal elastic connector: (a) massless rotational spring; (b) internal hinge; (c) massless translational spring; and (d) internal shear guide.

principle of fracture mechanics and given by [2] as

$$K_T = \frac{1}{c} = 5.346\frac{h}{EI}f\left(\frac{a}{h}\right), \tag{32}$$

where h and a are the thickness of the beam and the depth of the crack, respectively; and $f(a/h)$ is a nondimensional parameter determined by the crack geometry [2]

$$f\left(\frac{a}{h}\right) = 1.8624\left(\frac{a}{h}\right)^2 - 3.95\left(\frac{a}{h}\right)^3 + 16.37\left(\frac{a}{h}\right)^4 - 37.226\left(\frac{a}{h}\right)^5 + 76.81\left(\frac{a}{h}\right)^6 - 126.9\left(\frac{a}{h}\right)^7 + 172\left(\frac{a}{h}\right)^8 - 143.97\left(\frac{a}{h}\right)^9 + 66.56\left(\frac{a}{h}\right)^{10}. \tag{33}$$

Eq. (33) requires that the crack is open, which is not always true. As a matter of fact, the transverse crack can also open and close regularly (breath), or always close depending on the different loads applied on the beam, as discussed in details by Chondros et al. [28,29]. In such cases, more complicated models such as the breathing crack model [28,29] should be used.

By using the rotational spring model, only the slope of the beam is discontinuous at this point. Considering the rotation-moment relationship of the spring, we have

$$\Delta W'(x_i) = \frac{EI}{K_{Ti}}W''(x_i). \tag{34}$$

Cautions should be taken in using Eq. (34) to simulate the effect of a transverse crack because it is derived based on a few assumptions aforementioned. In the case that those assumptions are not valid, using Eq. (34) can lead to gross errors. When K_{Ti} is zero, we have an internal hinge in the beam (Fig. 5(b)). In this case, the slope discontinuity cannot be obtained through Eq. (34). Instead, we have

$$W''(x_i) = 0. \tag{35}$$

The translational spring is used to simulate the local transverse flexibility induced by a crack (Fig. 5(c)). This spring introduces a discontinuity of deflection at x_i as

$$\Delta W(x_i) = \frac{EI}{K_{Si}}W'''(x_i). \tag{36}$$

Specifically, if the stiffness K_{Si} is zero (Fig. 5(d)), we have a case of internal shear guide (shear free)

$$W'''(x_i) = 0. \tag{37}$$

At this point, it can be found that all the discontinuities discussed above can be expressed by the applied load and boundary values of the modal displacement.

3.4. Boundary conditions

As aforementioned, the boundaries are nothing but discontinuity points at the ends of the beam. General boundary conditions shown in Fig. 2 can be obtained by combining an elastic translational spring (Fig. 4(a)) and an elastic rotational spring (Fig. 4(c)). In such a case, all four discontinuities on the boundary are nonzero. While for the common boundary conditions listed in Table 1, only two are nonzero.

Table 1
Common boundary conditions for Euler–Bernoulli beams

Support type	Zero terms	Nonzero terms
Fixed	W, W'	W'', W'''
Pinned	W, W''	W', W'''
Free	W'', W'''	W, W'
Guided	W', W'''	W, W''

In the previous sections, the discontinuity terms at internal discontinuity points have been expressed in term of the discontinuity terms at the boundary point in a recursive formula. Combining Table 1 and the expressions of discontinuities obtained above in term of boundary values of the modal displacement, only two unknowns remain in the modal displacement, which can be easily determined by boundary conditions at the right end of the beam. As a result, tremendous effort of computation and cost associated with dynamic analysis of beams with discontinuities can be saved.

4. Application examples

To demonstrate the efficiency and applicability of the proposed method, vibration of Euler–Bernoulli beams with various commonly encountered discontinuities is solved in this section.

4.1. Vibration of cantilever beam using lead–zirconate–titanate (PZT) actuator

PZT ceramic patch is lightweight and thin piezoelectric material, which can be used as actuators and sensors in smart structures [24]. In Fig. 6, a PZT patch is externally bonded to a cantilever beam as an actuator. Two concentrated bending moments generated by applying a proper voltage to the PZT patch are applied to the beam at the ends of the PZT patch, as shown by Wang and Wang [24] (Fig. 6). In the case of harmonic vibration, the modal displacement of the cantilever beam can be written as

$$W(x) = \frac{W''(0)}{\lambda^2} S_2(\lambda x) + \frac{W'''(0)}{\lambda^3} S_3(\lambda x) + \frac{M_0}{EI\lambda^2} S_2(\lambda(x - x_1))H(x - x_1) - \frac{M_0}{EI\lambda^2} S_2(\lambda(x - x_1 - l))H(x - x_1 - l), \tag{38}$$

where M_0 is the moment applied to the beam by the PZT actuator; x_1 is the location of the left end of the PZT patch; l is the length of the actuator. Note that only two unknowns, i.e., $W''(0)$ and $W'''(0)$, in Eq. (38), which can be easily determined by the boundary condition at the free end

$$W'''(L) = 0, \quad W''(L) = 0. \tag{39}$$

The dynamic response of the beam under harmonic unit bending moment applied by the PZT actuator with $\lambda = 2$ and $l = 0.02\,\mathrm{L}$ is presented in Fig. 7. Fig. 7(a) shows that the location of the actuator has significant effect on the deformation of the beam. The deflection of the beam is larger if the actuator is closer to the fixed end of the beam. This trend is further confirmed by Fig. 7(b), in which the curvature shapes of beam are obtained for three different actuator locations. Except at the location of the actuator where the curvature is much higher due to the bending moment applied by the actuator, the curvature is higher when the actuator is closer to the fixed end. Such a phenomenon suggests that in order to achieve better excitation effect, the PZT actuator should be placed as close to the fixed end in a cantilever configuration as possible.

4.2. Free vibration of cantilever beam with multiple-cracks

As aforementioned, the free vibration of a beam with multiple cracks has been studied extensively [1–7,25–27] due to its application in damage detection. By using Eq. (20), the modal shape of the beam is

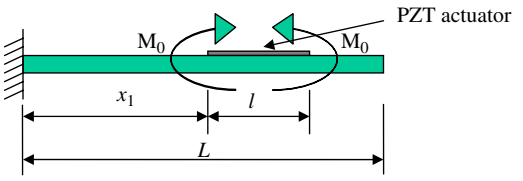

Fig. 6. Cantilever beam excited by a PZT actuator.

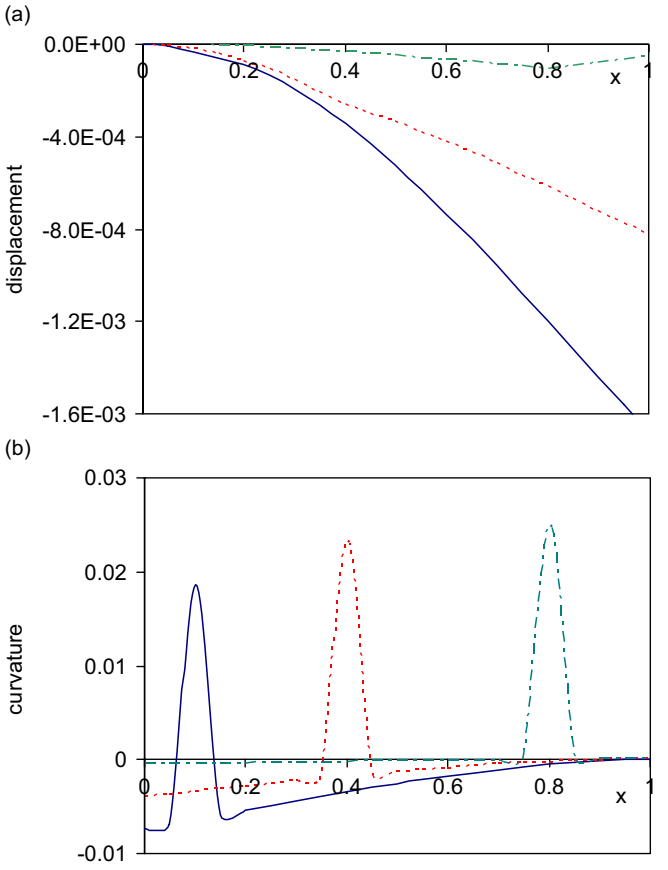

Fig. 7. Dynamic response of the cantilever beam under PZT actuator: (a) modal displacement; and (b) modal curvature. ——— $x_1 = 0.1$, - - - - - $x_1 = 0.4$, -·-·-·- $x_1 = 0.8$.

derived as

$$W(x) = W(0)S_0(\lambda x) + \frac{W'(0)}{\lambda}S_1(\lambda x) + \frac{W''(0)}{\lambda^2}S_2(\lambda x) + \frac{W'''(0)}{\lambda^3}S_3(\lambda x) + \sum_{i=1}^{n}\frac{EIW''(x_i)}{K_{Ti}\lambda}S_2(\lambda(x-x_i))H(x-x_i). \tag{40}$$

In Eq. (40), only four discontinuities at the left boundary need to be determined. For a cantilever beam with two cracks studied by Ruotolo et al. [26], Eq. (40) can be simplified as

$$W(x) = \frac{W''(0)}{\lambda^2}S_2(\lambda x) + \frac{W'''(0)}{\lambda^3}S_3(\lambda x) + \frac{EIW''(x_1)}{K_{T1}\lambda}S_2(\lambda(x-x_1))H(x-x_1) + \frac{EIW''(x_2)}{K_{T2}\lambda}S_2(\lambda(x-x_2))H(x-x_2). \tag{41}$$

Considering boundary conditions at the free end (Eq. (39)), we have

$$\begin{pmatrix} a_{11} & a_{12} \\ a_{21} & a_{22} \end{pmatrix} \begin{pmatrix} W''(0) \\ W'''(0) \end{pmatrix} = \begin{pmatrix} 0 \\ 0 \end{pmatrix}, \tag{42}$$

where $k_i = ET/K_{Ti}$ and

$$\begin{aligned}
a_{11} &= S_2''(\lambda L) + k_1\lambda S_1''(\lambda(L-x_1))S_2''(\lambda x_1) + k_2\lambda S_1''(\lambda(L-x_2))\big(S_2''(\lambda x_2) + k_1\lambda S_1''(\lambda(x_2-x_1))S_2''(\lambda x_1)\big),\\
a_{12} &= S_2''(\lambda L)\frac{1}{\lambda} + k_1 S_1''(\lambda(L-x_1))S_3''(\lambda x_1) + k_2 S_1''(\lambda(L-x_2))\big(S_3''(\lambda x_2) + k_1\lambda S_1''(\lambda(x_2-x_1))S_3''(\lambda x_1)\big),\\
a_{21} &= S_2'''(\lambda L) + k_1\lambda S_1'''(\lambda(L-x_1))S_2''(\lambda x_1) + k_2\lambda S_1'''(\lambda(L-x_2))\big(S_2''(\lambda x_2) + k_1\lambda S_1''(\lambda(x_2-x_1))S_2''(\lambda x_1)\big),\\
a_{22} &= S_2'''(\lambda L)\frac{1}{\lambda} + k_1 S_1'''(\lambda(L-x_1))S_2''(\lambda x_1) + k_2 S_1'''(\lambda(L-x_2))\big(S_2''(\lambda x_2) + k_1\lambda S_1''(\lambda(x_2-x_1))S_2''(\lambda x_1)\big).
\end{aligned} \tag{43}$$

The natural frequency of the beam given by the root of the following equation:

$$a_{11}a_{22} - a_{12}a_{21} = 0. \tag{44}$$

The natural frequencies of the beam in Fig. 8 was obtained by Ruotolo et al. [26] by using the so-called "continuous model". The following properties are used in the calculation: length $L = 0.8$ m, rectangular cross-section with width $b = 0.02$ m and height $h = 0.02$ m, a first crack with position $x_1 = 0.12$ m and depth $a_1 = 2$ mm, a second crack with variable position from the clamped to the free end and a depth of 2, 4, and 6 mm. The first three frequencies of this beam (ω) are obtained by Eq. (44) and normalized by the frequencies without crack (ω_0) for different location of x_2 and presented in Fig. 9. As a comparison and verification, the values obtained by Ruotolo et al. [26] are also presented in Fig. 9. It can be seen that excellent agreements of the present solution and the ones in Ref. [26] have been achieved for all the cases studied.

4.3. Driving-point anti-resonance frequency of cracked beam

Driving-point anti-resonance frequency has gained attention recently for its potential application in damage detection [30,31]. Bamnious, Douka and Trochidis [31] demonstrated that a crack in a beam could be identified by a sharp jump in the slope of the curve of the driving point anti-resonance frequency verse the measuring position. To obtain the driving-point anti-resonance frequencies of a cracked cantilever beam shown in Fig. 10(a), a forced vibration problem shown in Fig. 10(b) is first solved by Bamniou et al. [31], based on which the anti-resonance frequency is then obtained. The commonly used approach was adopted in

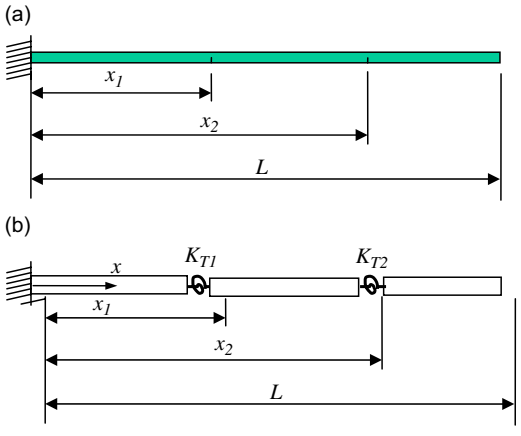

Fig. 8. Cantilever beam with two cracks: (a) cracked cantilever beam; (b) equivalent rotational spring model.

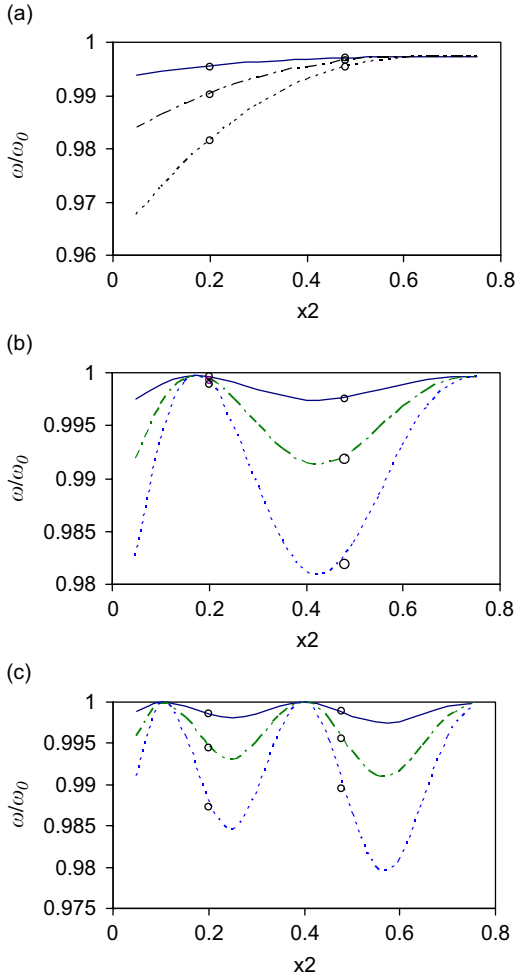

Fig. 9. Comparison of natural frequencies of a cantilever beam with two cracks (a) First natural frequency; (b) second natural frequency; and (c) third natural frequency. —— $a/h = 0.1$, -·-·-·- $a/h = 0.2$, - - - - $a/h = 0.3$, ○ Ref. [26].

Bamnious et al. [31], which led to determination of 12 unknown coefficients simultaneously. If the present solution in Eq. (20) is used, the modal displacement is simplified as

$$W(x) = \frac{W''(0)}{\lambda^2} S_2(\lambda x) + \frac{W'''(0)}{\lambda^3} S_3(\lambda x) + \frac{W''(x_1)}{K_\tau \lambda^2} S_2(\lambda(x - x_1)) H(x - x_1) + \frac{P}{EI\lambda^2} S_3(\lambda(x - x_2)) H(x - x_2). \tag{45}$$

In this way, only two unknown coefficients exist which can be determined by the boundary conditions at the free end given by Eq. (39). The driving-point anti-resonance of the beam is then obtained by the location of peak values on the impedance-frequency curve.

To avoid the tedious task of calculating the whole impedance curve, an alternative method is proposed in the present study, which can provide the driving-point anti-resonance frequency of a cracked beam directly and accurately. Note that the driving-point anti-resonance frequencies correspond to the mode frequencies of the structure with the driving point degree-of-freedom restrained to ground. Therefore, to find

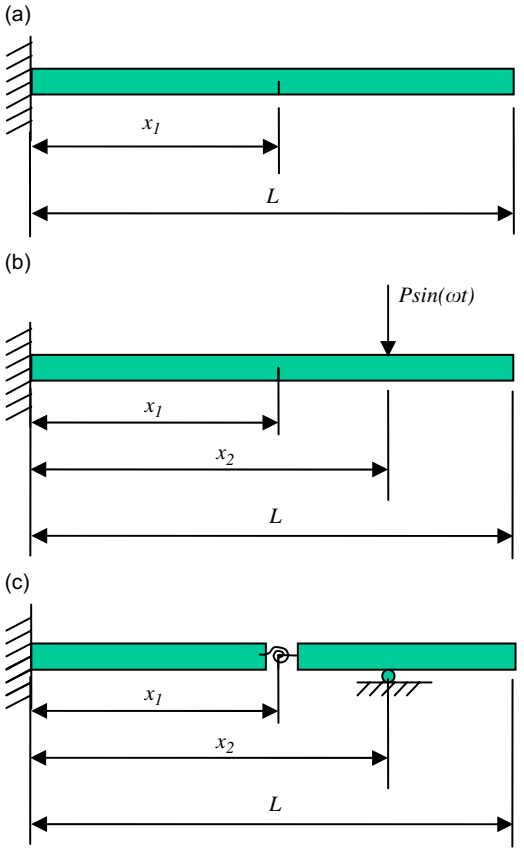

Fig. 10. Driving-point anti-resonance of a cracked cantilever beam: (a) cracked cantilever beam; (b) forced vibration model; and (c) equivalent free vibration model.

the driving-point anti-resonance frequencies of a cracked cantilever beam of Fig. 10(a) at x_2 is equivalent to obtain the natural frequencies of the same beam with a roller support at x_2 (Fig. 10(c)). In this case, the modal shape is given by

$$W(x) = \frac{W''(0)}{\lambda^2} S_2(\lambda x) + \frac{W'''(0)}{\lambda^3} S_3(\lambda x) + \frac{EIW''(x_1)}{K_T \lambda^2} S_2(\lambda(x - x_1))H(x - x_1) + \frac{W'''(x_2)}{EI\lambda^2} S_3(\lambda(x - x_2))H(x - x_2). \quad (46)$$

To determine the three unknown coefficients in Eq. (46), besides two boundary conditions at the free end given by Eq. (39), the following condition at x_2 is employed

$$W(x_2) = 0. \quad (47)$$

The first natural frequencies obtained by the above solution and first driving-point anti-resonance frequencies experimentally measured by Barmnios et al. [31] for a plexigal cantilever beam of which $L = 35\,\text{mm}$, $b \times \text{h} = 2 \times 2\,\text{cm}$ are presented in Fig. 11. A saw-cut with depth a at 15 cm from the fixed end is used to simulate damage. Three different depths of the crack are considered in Fig. 11, i.e., $a/h = 0.4$, $a/h = 0.6$, and $a/h = 0.8$. It can be observed that the anti-resonance frequency of the beam decreases with the size of the crack. An interesting feature of Fig. 11 is that there is a jump in the slope of the curve of the driving-point anti-resonance frequency verse the location. Such a jump indicates the existence and location of the crack on the beam. This phenomenon is further demonstrated in Fig. 12 in which the change of anti-resonance

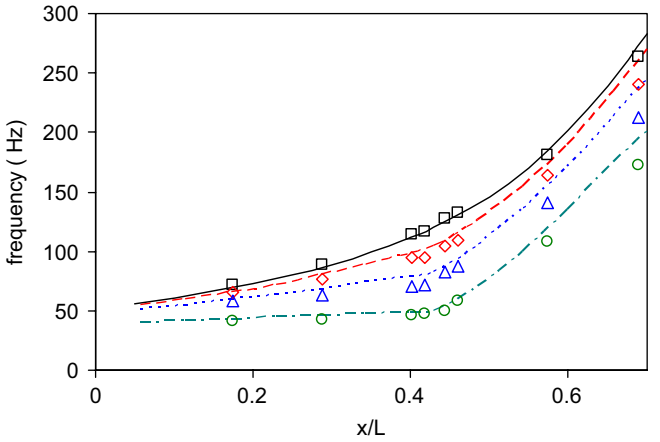

Fig. 11. Comparison of driving-point anti-resonance frequency obtained by the present theoretical method and the experimental data in Ref. [31]. □ experimental, $a/h = 0$; ——— theoretical, $a/h = 0$; ◇ experimental, $a/h = 0.4$; - - - - - theoretical, $a/h = 0.4$; △ experimental, $a/h = 0.6$; - - - - - theoretical, $a/h = 0.6$; ○ experimental, $a/h = 0.8$; - · - · - and theoretical, $a/h = 0.8$.

frequencies induced by the crack is presented with the location of the driving-point for the first three modes. As expected, there is a sharp peak appearing at the location of the crack on all these curves corresponding to the different magnitudes of the damage (i.e., the depth of crack). It can be observed that the reduction of anti-resonance frequencies is higher if the crack size is larger. Such a relationship may be used to quantify the size of crack.

5. Conclusions

In the study, vibration of an Euler–Bernoulli beam with various additional elements is addressed, and applications of the solution to smart structures modeling and damage detection of beam-type structures are demonstrated. Various discontinuities can be induced to the modal displacement of the beam at the locations of these additional elements. Unlike the commonly used approach in the literature, only a single function is used to describe the modal displacement of the whole beam by using Heaviside's function to account for discontinuities. The obtained modal displacement consists of the basic modal shapes induced by the discontinuities at the discontinuity points. This solution can account for arbitrary number and type of discontinuity points on a beam by expressing the discontinuities in term of boundary values of the modal displacement through a recursive way. Consequently, the complexity of the vibration is reduced to the same order of a beam without any discontinuity points.

Three examples are further presented in this study to verify and demonstrate the efficiency and applicability of the present method. The harmonic vibration of a cantilever beam with smart materials (e.g., PZT actuator) shows that the actuator should be placed as close as possible to the fixed end of the beam in order to achieve maximized excitation result. An exact analytical method is also presented to calculate the driving-point anti-resonance frequency of cracked beam. It has been shown that the crack location and size may be determined by the anti-resonance frequency.

It is very difficult to present and compare results for all cases of the dynamic behavior of smart structures with flaws because there are so many parameters that can be varied in the vibration of the structures. More complicated situations of dynamic behavior of this type of damaged structures, such as coupled flexural and longitudinal vibration, will be subjects of our future study. Nevertheless, the general approach and solution presented in this study provides an efficient tool to study and analyze the dynamic behavior of beam-type of smart structures.

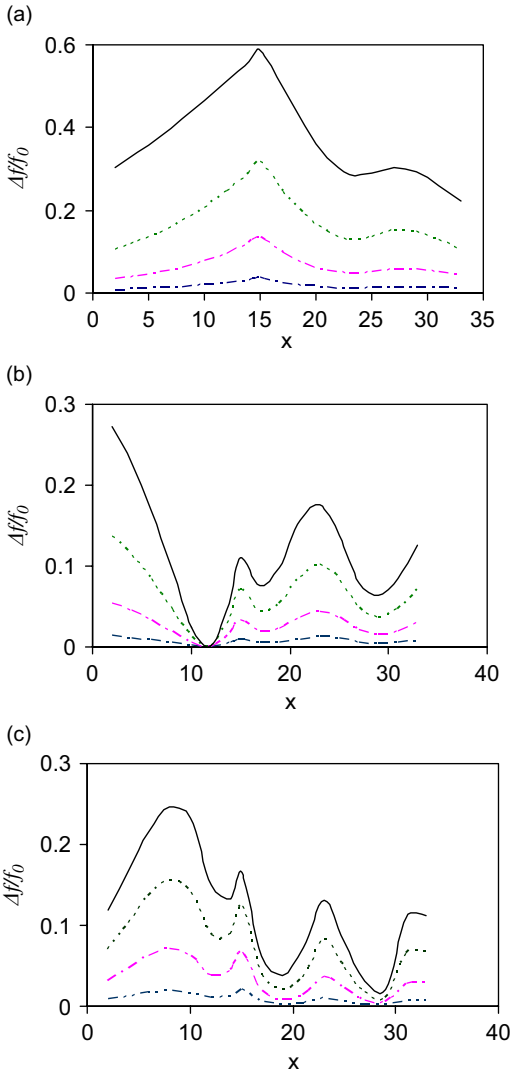

Fig. 12. Shift of driving-point anti-resonance frequency due to the presence of crack: (a) first mode; (b) second mode; and (c) third mode. — · · — · · $a/h = 0.2$, - · - · - · $a/h = 0.4$, - - - - $a/h = 0.6$, ——— $a/h = 0.8$.

Acknowledgments

The authors want to thank the partial financial support provided by the Air Force Office of Scientific Research (AFOSR) (Contract No. FA9650-04-C-0078).

References

[1] S.W. Doebling, C.R. Farrar, M.B. Prime, Summary review of vibration-based damage identification methods, *Shock and Vibration Digest* 30 (1998) 91–105.
[2] S.A. Paipetis, A.D. Dimarogonas, *Analytical Methods in Rotor Dynamics*, Elsevier Applied Science, London, 1986.
[3] P.F. Rizos, N. Aspragatos, A.D. Dimarogonas, Identification of crack location and magnitude in a cantilever beam from the vibration modes, *Journal of Sound and Vibration* 138 (1990) 381–388.
[4] E.I. Shifrin, R. Ruotolo, Natural frequencies of a beam with an arbitrary number of cracks, *Journal of Sound and Vibration* 223 (1999) 409–423.

[5] Q.S. Li, Free vibration analysis of non-uniform beams with an arbitrary number of cracks and concentrated masses, *Journal of Sound and Vibration* 252 (2001) 509–525.
[6] N.T. Khibm, T.V. Lien, A simplified method for natural frequency analysis of a multiple cracked beam, *Journal of Sound and Vibration* 245 (2001) 737–751.
[7] A.D. Dimarogonas, Vibration of cracked structure: a state of the art review, *Engineering Fracture Mechanics* 55 (1996) 831–857.
[8] T.G. Chondros, A.D. Dimarogonas, Dynamics sensitivity of structures to cracks, *Journal of Vibration, Acoustics, Stress and Reliability in Design* 111 (1989) 2521–2556.
[9] T.G. Chondros, The continuous crack flexibility method for crack identification, *Fatigue & Fracture of Engineering Materials & Structures* 24 (2001) 643–659.
[10] C.N. Bapat, C. Bapat, Natural frequencies of a beam with non-classical boundary conditions and concentrated masses, *Journal of Sound and Vibration* 112 (1987) 128–177.
[11] A. Posiadala, Free vibrations of uniform Timoshenko beams with attachments, *Journal of Sound and Vibration* 204 (1997) 359–369.
[12] J.S. Wu, H.M. Chou, Free vibration analysis of a cantilever beam carrying any number of elastically mounted point masses with the analytical-and-numerical-combined method, *Journal of Sound and Vibration* 213 (1998) 317–332.
[13] S.Q. Lin, C.N. Bapat, Free and forced vibration of a beam supported at many locations, *Journal of Sound and Vibration* 142 (1990) 254–342.
[14] A. Kameswara Rao, Frequency analysis of clamped–clamped uniform beams with intermediate elastic support, *Journal of Sound and Vibration* 133 (1989) 502–509.
[15] K. Kukla, B. Posiada, Free vibrations of beams with elastically mounted masses, *Journal of Sound and Vibration* 175 (1994) 557–564.
[16] Q.S. Li, Torsional vibration of multi-step non-uniform rods with various concentrated elements, *Journal of Sound and Vibration* 260 (2003) 637–651.
[17] A. Yavari, S. Sarkani, E.T. Moyer, On applications of generalized functions to beam bending problems, *International Journal of Solids and Structures* 37 (2000) 5676–5705.
[18] A. Yavari, S. Sarkani, J.N. Reddy, Generalized solutions of beams with jump discontinuities on elastic foundations, *Archive of Applied Mechanics* 71 (2001) 625–639.
[19] M. Gürgöze, On the eigenfrequencies of a cantilever beam with attached tip mass and a spring–mass system, *Journal of Sound and Vibration* 190 (1996) 149–162.
[20] J.S. Wu, D.W. Chen, Bending vibrations of wedge beams with any number of point masses, *Journal of Sound and Vibration* 262 (2003) 1073–1090.
[21] H. Abromovich, O. Hamburger, Vibration of a uniform cantilever Timoshenko beam with translational and rotational springs and with a tip mass, *Journal of Sound and Vibration* 154 (1992) 67–80.
[22] L. Ercoli, P.A.A. Laura, Analytical and experimental investigation on continuous beams carrying elastically mounted masses, *Journal of Sound and Vibration* 114 (1987) 519–533.
[23] H. Qiao, Q.S. Li, G.Q. Li, Vibratory characteristics of flexural non-uniform Euler–Bernoulli beams carrying an arbitrary number of spring–mass systems, *International Journal of Mechanical Sciences* 44 (2002) 725–743.
[24] B.T. Wang, C.C. Wang, Feasibility analysis of using piezoceramic transducers for cantilever beam model testing, *Smart Materials and Structures* 6 (1997) 106–116.
[25] B. Binici, Vibration of beams with multiple open cracks subjected to axial force, *Journal of Sound and Vibration* 287 (2005) 277–295.
[26] R. Ruotolo, C. Surace, C. Mares, Theoretical and experimental study of the dynamic behaviour of a double-cracked beam, *Proceedings of 14th International Modal Analysis Conference*, Dearborm, Michigan, USA, 1996, pp. 1560–1564.
[27] O. Song, T.W. Ha, L. Librescu, Dynamics of anisotropic composite cantilevers weakened by multiple transverse open cracks, *Engineering Fracture Mechanics* 70 (2003) 105–123.
[28] T.G. Chondros, A.D. Dimarogonas, J. Yao, Vibration of a beam with a breathing crack, *Journal of Sound and Vibration* 239 (2001) 57–67.
[29] T.G. Chondros, A.D. Dimarogonas, J. Yao, Longitudinal vibration of a bar with a breathing crack, *Engineering Fracture Mechanics* 61 (1998) 503–518.
[30] M. Dilena, A. Morassi, The use of antiresonaces for crack detection in beams, *Journal of Sound and Vibration* 276 (2004) 195–214.
[31] Y. Bamnios, E. Douka, A. Trochidis, Crack identification in beam structures using mechanical impedance, *Journal of Sound and Vibration* 256 (2002) 287–297.